Measurements of visible forbidden lines and ion distributions of tungsten highly charged ions at the LHD

D. Kato[1], H.A. Sakaue[1], I. Murakami[1], M. Goto[1], S. Morita[1], N. Nakamura[2], F. Koike[3], A. Sasaki[4], X.-B. Ding[5], C.-Z. Dong[5]

[1] National Institute for Fusion Science, Toki, Gifu 509-5292, Japan

[2] ILS, The University of Electro-Communications, Tokyo 182-8585, Japan

[3] Faculty of Science and Technology, Sophia University, Tokyo 102-8554, Japan

[4] Japan Atomic Energy Agency, Kyoto 619-0215, Japan

[5] Northwest Normal University, Lanzhou 730070, China

Abstract: Visible lines, which are presumably associated with forbidden lines from tungsten highly charged ions, were clearly observed in a spectrum of 370 – 410 nm recorded shortly after a tungsten pellet injection at the LHD. One of the measured lines has been assigned to a magnetic-dipole (M1) line of the ground-term fine-structure transition of W^{26+}. Photon emission was observed at 44 lines of sight divided along the vertical direction of a horizontally elongated poloidal cross section of the LHD plasma. The line-integrated intensity of the lines along each line of sight indicates peaked profiles near the plasma center, while visible line emissions of neutral hydrogen and helium recoded in the same sampling time have a maximum located in the peripheral region of the poloidal cross section.

1. Introduction

One of important issues concerning steady state sustainment of magnetically confined plasmas (MCPs) is distribution of impurity ions in the MCPs and radiation powers by the impurity ions. Since tungsten divertors will be used in ITER, the primary element of heavy impurity ions would be tungsten. Thus, strong emission lines of highly ionized tungsten ions in core plasmas have intensively been measured in short wavelength regions, e.g. extreme-ultra-violet (EUV) [1-3].

Visible forbidden lines from highly charged ions (HCIs) of heavy elements provide new diagnostics means to study behaviors of heavy impurity ions in the fusion plasmas. High-resolution spectroscopy and fiber optics are available in the visible region, which enable precise plasma diagnostics and advantageous for preventing detection systems from neutron damage. Since fine-structure splitting of heavy ions such as tungsten increases rapidly with ionization degrees, forbidden lines of highly ionized ions could be observed in visible ranges. Spectral data for the visible forbidden-lines of highly charged tungsten ions, however, are very limited [4]. An M1 transition of

Ti-like W^{52+} ($3d^4$) $^5D_3$ - $^5D_2$ has been known by numbers of studies by means of Electron-Beam-Ion-Traps (EBITs) ([5] and references therein). Recently, Komatsu [6] and Watanabe [7] found a strong visible M1 line of Cd-like W^{26+} in the EBITs. The line has been identified as the ground-term fine-structure transition of $4f^2$ $^3H_5$ - $^3H_4$ [8]. In the present work, we conducted measurements of visible lines from the tungsten HCIs in the Large Helical Device (LHD) using solid pellet injection techniques [9].

2. LHD Experiment

Discharges for present measurements were started with electron cyclotron heating followed by hydrogen neutral beam injection (NBI) heating. In steady state, the maximum electron temperature is 2 - 3 keV at the plasma center. Then, a solid pellet containing tungsten was injected into background hydrogen plasmas. Two kinds of pellets were used in the present experiments. One is so called as Tracer-Encapsulated Solid Pellet (TESPEL) [10]. The TESPEL is a double-layered impurity pellet, which consists of polystyrene polymer as an outer shell (diameters of 400 - 900 μmφ) and tracer particles as an inner core. We used another impurity pellet [11] also (henceforth, we denote this pellet as the impurity pellet), which has a cylindrical carbon shell (diameter of 1.2 μmφ) with tin coating. Tungsten powders are contained inside a hole at the center of the carbon shell. The TESPEL and the impurity pellet are injected at speeds of 200 - 500 m/s and 30 - 300 m/s by specially designed pellet injectors, respectively.

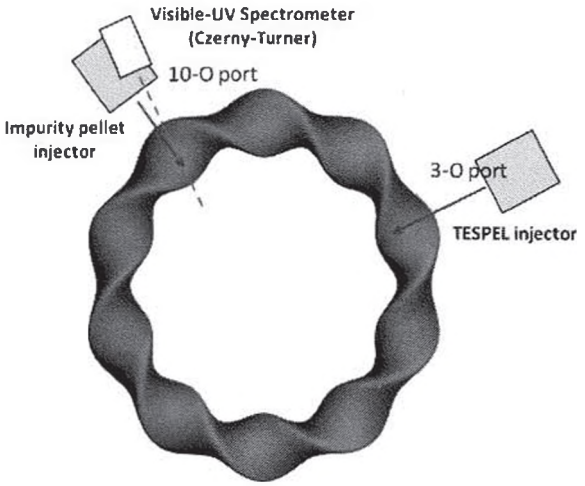

Figure 1: A top view of helical plasmas, pellet injectors and a visible-UV spectrometer.

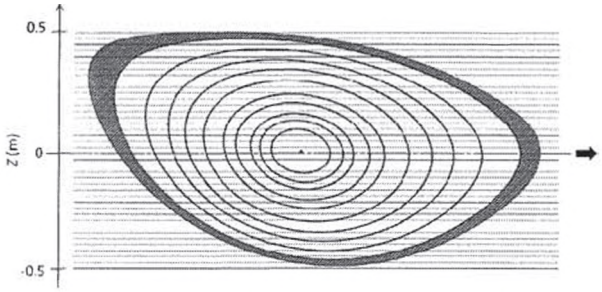

Figure 2: Horizontally elongated poloidal cross section and lines of sight. Shaded area represents the peripheral region. The black allow indicates the viewing direction.

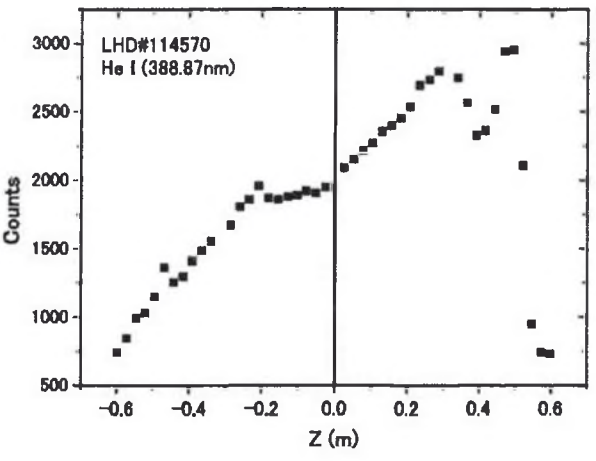

Figure 3: Vertical distribution of line-integrated intensity for a He I line.

Time-resolved (sampling times for 38 and 140 ms at every 100 and 250 ms, respectively) measurements were conducted using Czerny-Turner visible-UV spectrometers equipped with CCD detectors. Figure 1 shows a viewing port as well as two pellet injection ports. Using an optical fiber array, photon emission was observed at 44 lines of sight divided along the vertical direction (Z) of a horizontally elongated poloidal cross section of a helical plasma, as shown in Fig. 2. It is noted that the poloidal cross section is asymmetric with respect to $Z = 0$, because the cross section is tilted a little from the normal direction. This asymmetry manifests itself in vertical distributions of line-integrated intensities (along each line of sight) of emission lines in peripheral regions of the poloidal cross section [12]. Figure 3 illustrates a typical example with the He I line (388.87 nm) emitted in the peripheral region.

3. Results and Discussion

3.1 Observation of visible M1 lines of W HCIs at the LHD

Figure 4 shows a series of CCD images of line emissions obtained in three successive sampling time frames before (f14: 3550 - 3690 ms) and after (f15: 3800 - 3940 ms and f16: 4050 – 4190 ms) the TESPEL injection (3800 ms). 3.32×1017 tungsten atoms were contained in this TESPEL core. After the TESPEL injection, central electron temperatures decrease due to power exhaust by pellet ablation and ionization and line emission of tungsten ions, while the NBI heating is kept turned on. The line emissions from highly charged tungsten ions are anticipated only for the instant before the electron temperature decreases to so low that the ions cannot be created appreciably. In the present measurement, before the TESPEL injection, i.e. f14, the maximum electron temperature exceeds 2 keV at the plasma center. Then, the electron temperatures decreased down to 350 eV or lower at the beginning of f16. Strong line emissions peaked at vertical positions around $Z = 0.5$ and 0.25 are from peripheral regions of the poloidal cross sections (see Fig. 3). However, a distinct emission profile is found for the time frame just after the TESPEL injection, i.e. f15; there is another peak centered around $Z = 0$. To see this emission component separately, the CCD image of f14 is subtracted from that of f15 as shown in the upper panel of Fig. 5.

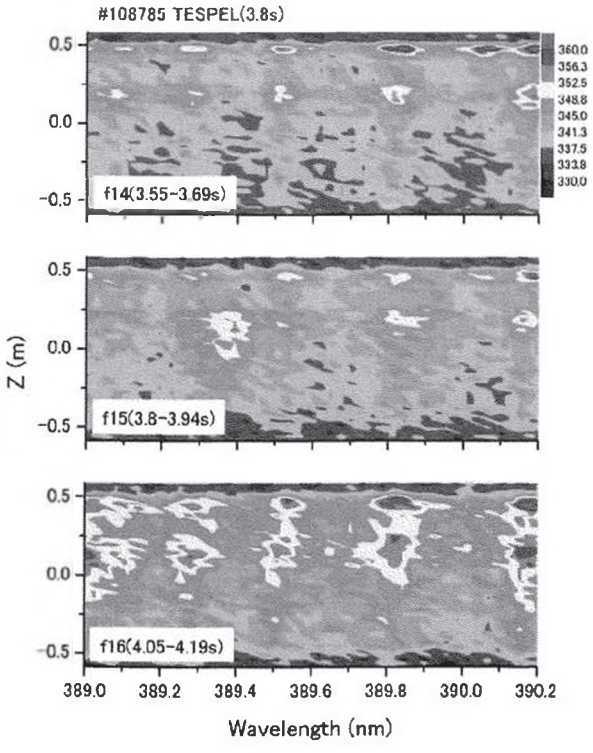

Figure 4: CCD images of line emissions in a visible

range obtained in three successive sampling time frames before (f14: 3550 - 3690 ms) and after (f15: 3800 - 3940 ms and f16: 4050 – 4190 ms) the TESPEL injection.

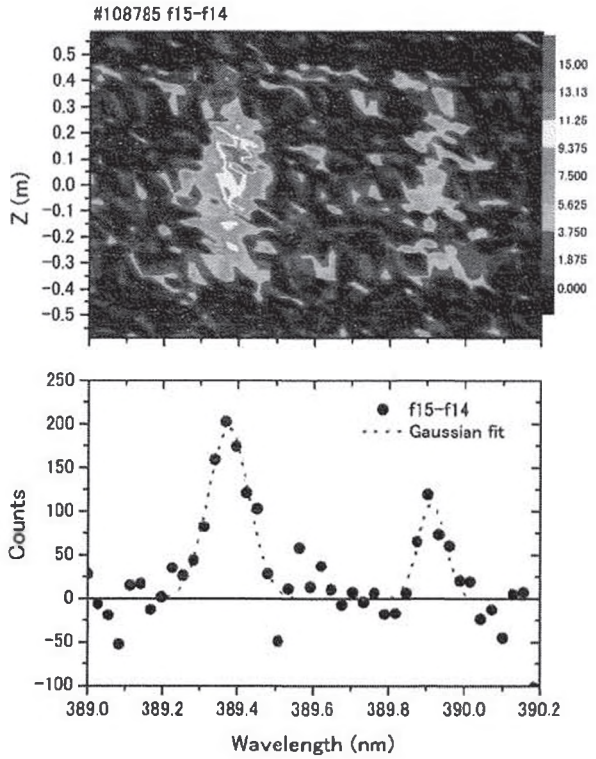

Figure 5: A spectrum of emission lines from highly charged tungsten ions observed at LHD (shot #108785). The scale on the right hand side of the top panel shows photon counts per pixel of the CCD detector. See text for details.

Table 1: Measured wavelengths (nm) and references. Numbers in parentheses are uncertainties.

Peak	Present	EBIT	Theory
A	389.37(4)	389.41(6) [6] 389.35(3) [7]	388.43 [8]
B	389.91(4)	389.89(6)[13]	-

In the lower panel, two peaks, which are absent in the spectrum measured during the former sampling time frame, i.e. f14, are apparent. Gaussian fitting of the two peaks gives central wavelengths of 389.37 nm (Peak A) and 389.91 nm (Peak B), respectively. The results are compared with available references in Table 1. Uncertainties of the central wavelengths are totally about 0.04 nm. Although standard deviations of the central wavelengths (the confidence level is 63.8 %) are less than 0.01 nm, the dominant uncertainty is due to errors in wavelength calibration which has been done with the hydrogen Balmer series of lines emitted in the last phase of the same discharge. The present wavelength for Peak A is identical to within the uncertainty a tungsten line measured in various EBITs [6, 7]. That line has been identified due to a ground-term M1 transition of W^{26+} ($4f^2$) $^3H_5$ - $^3H_4$ by large-scale multi-configuration Dirac-Fock calculations [8]. Peak B is presumably due to a line emission from W^{24+}, because an emission line with the almost identical wavelength has been observed recently with a compact EBIT (CoBIT) [13]. Both of the lines are absent in spectra of sampling times of f16 where the electron temperatures are lower than 350 eV.

3.2 Ionization equilibrium and radial distribution of W^{26+}

Figure 6 shows fractional abundances of tungsten ions of different charge states as a function of electron temperature calculated by using a collisional-radiative (CR) model [14] for an electron density of 1020 /m3. The fractional abundance of W^{26+} ions is peaked around 400 - 500 eV according to this calculation. It is

noted that different models give significantly different fractional abundances especially at electron temperatures lower than 1 keV, mainly because of uncertainties in rate coefficients of atomic processes involved in the models. Using an electron temperature profile measured by the Thomson scattering system at the LHD, a radial distribution of W^{26+} ions is calculated as shown in Fig. 7. The radial distribution has a peak at radial positions apart from the plasma center (major radius R = 3.6 m) in a case that the electron temperature profile measured at t = 3933 ms (the end of the time frame f15) is used. This seems inconsistent with the M1 intensity profile of W^{26+} ions which is peaked around the plasma center. It is noted that an electron temperature profile at an earlier time has a higher central value, the peak position of the W^{26+} fractional abundance would be even far apart from the plasma center with such the temperature profile.

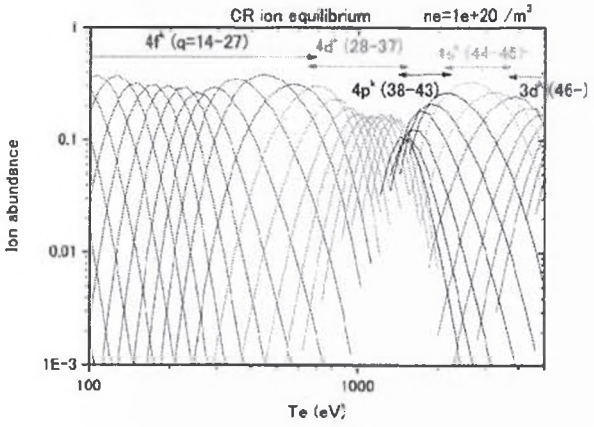

Figure 6: Fractional abundance of tungsten ions as a function of electron temperature calculated by using a collisional-radiative (CR) model [14] for an electron density of 10^{20} /m^3.

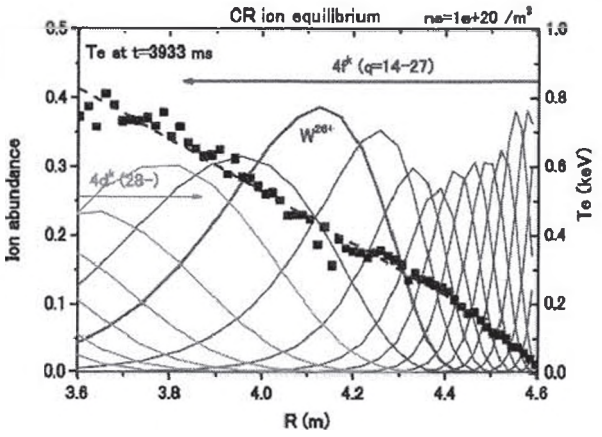

Figure 7: Radial distribution of W^{26+} ions in the LHD plasmas and an electron temperature profile measured by the Thomson scattering system.

Ion transports give significant effects in the ion fractional abundance. Suppose that a high-temperature core plasma acquires a significant in-flux of lower charged ions in a time scale shorter than that required to achieve an ionization-equilibrium, the factional abundance of the lower charged ions in the core plasma would be enhanced. This has been known as a non-equilibrium ionization effect, since Post investigated this effect in terms of a scaled ion transport time [15], which is given by a product of electron densities and ion transport times limited by diffusion or convection. Apparent inconsistence found in this work between the measured M1 intensity profile and the calculated ion distribution may be ascribed to the ion transport effect, which will be addressed in our future studies.

3.3 New visible lines of W HCIs and comparison with EBIT spectra

We have conducted further measurements to seek other forbidden lines of tungsten HCIs in the visible range using another spectrometer which has a shorter focal length (30 cm) and a smaller F-number. In this measurement, tungsten was injected with the impurity pellet. Figure 8 shows electron temperature profiles measured before and after the pellet injection (about 4060 ms), central electron temperatures decrease rapidly, while two NBIs (#4 and #5) are turned on.

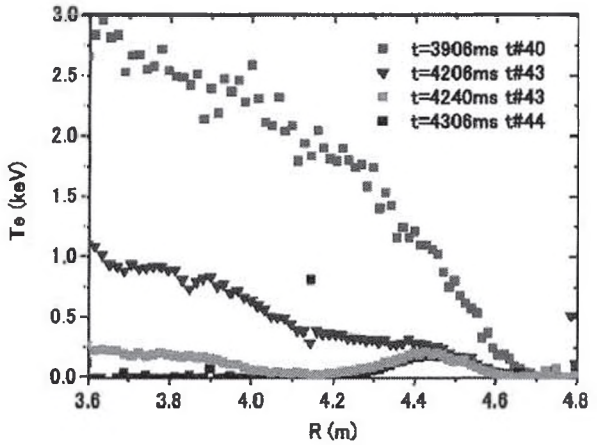

Figure 8: Variation of electron temperature profiles before and after a tungsten pellet injection (LHD#114570).

Figure 9 shows line-integrated spectra along a line of sight (Z = 2.6 cm) which passes through about the plasma center. These spectra were measured in three sampling time frames (t#40: 3900 – 3938 ms, t#43: 4200 – 4238 ms, and #t44: 4300 - 4338 ms), respectively. In the figure assignments of emission lines are also indicated. Most of prominent lines in the spectra of t#40 and t#44 can be assigned to those of the impurities inherent in the LHD, neutral hydrogen and helium atoms. Fe I lines appears in the spectrum of t#40 but not that of t#44. Fe contamination may be ascribed to sputtering from the first-wall of the main chamber made of stainless steels by bombardments of high-energy charge-exchange neutrals anticipated only for t#40. The hydrogen Balmer series is clearly seen in the spectrum of t#44, because of the lower central electron temperature as well as better statistics in photon counting (higher electron densities).

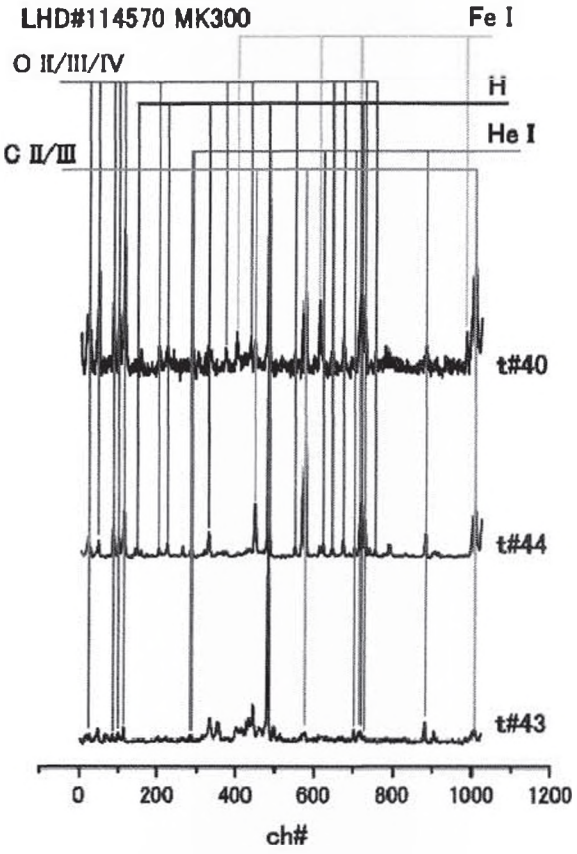

Figure 9: Line-integrated spectra along a line of sight (Z = 2.6 cm) through about the plasma center. The spectra are obtained in three sampling time frames (t#40: 3900 – 3938 ms, t#43: 4200 – 4238 ms, and #t44: 4300 - 4338 ms). The horizontal axis is channel number of a CCD detector.

There are still many unassigned lines remained in the

spectrum of t#43. In Fig. 10, the line-integrated spectra along two lines of sight are compared. One is the same as in Fig. 9, i.e. the line of sight which passes through about the plasma center, the other is that along a line of sight at a large vertical position (Z = 49.5 cm) of the horizontally elongated poloidal cross section. The later line of sight passes through a peripheral region of the poloidal cross section only (see Fig. 2). By comparing the two spectra, emission lines from the core plasma can be identified, which are indicated by arrows in the figure. Two of them (indicated by red arrows) are assigned to the previously identified M1 line of W^{26+} ($4f^2\ ^3H_5 - {}^3H_4$) and a visible line of W^{24+} ions, respectively. Other unassigned lines are presumably also visible lines of tungsten HCIs.

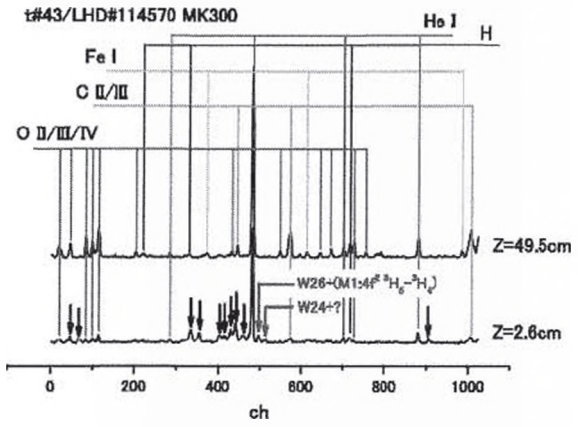

Figure 10: Line-integrated spectra along different lines of sight. Lower spectrum is the same as in Fig. 9, i.e. the line-integrated spectrum along the line of sight through about the plasma center, upper is that along the line at a large vertical position of the horizontally elongated poloidal cross section (Z = 49.5 cm, see Fig. 2).

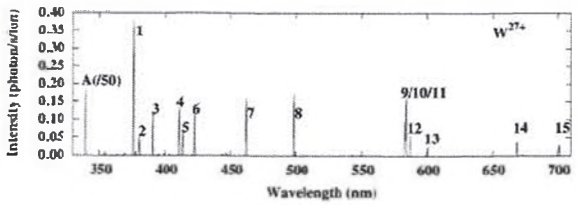

Figure 11: A synthetic spectrum of W^{27+} ions in an EBIT calculated by a collisional-radiative model [16]. Electron density of 10^{16} /m^3 and monochromatic electron beam energy of 830 eV are assumed for the EBIT. Intensity of line A is divided by 50.

Recently, quite a bit of spectral data for visible lines of the tungsten HCIs have been obtained by means of the CoBIT [13] which is very useful for analysis of the LHD spectra. However, it is not always straightforward to deduce the tungsten lines in LHD spectra by simply comparing with the CoBIT spectra. In the EBIT, trapped ions are excited by collisions with a quasi-monochromatic and unidirectional electron beam confined with a parallel magnetic field. A typical electron density obtained in the CoBIT is about 10^{16} /m^3, which is three or four orders of magnitude smaller than those in the LHD plasmas. Such large discrepancies in the electron density may give different population kinetics of fine-structure levels, which results in different emission line spectra. For instant, visible forbidden lines due to transitions in a fine-structure of an electronic excited level are hardly anticipated at low electron densities, unless the excited level is highly meta-stable. On the other hand, larger electron collision frequencies at higher electron

densities may quench the line emissions of longer life times, like the forbidden lines. Collisional-radiative (CR) models for detailed multiplet levels of the tungsten HCIs are required to address this issue. By collaboration with Chinese researchers, such a CR model for W^{27+} ions has been developed and electron density dependent variation of relative intensities of visible forbidden lines was investigated [16]. Figure 11 shows an example of calculated line spectra for W^{27+} ions in an EBIT assuming an electron density of 10^{16} /m^3 and a monochromatic electron beam energy of 830 eV. The strongest line A around 340 nm is identified as an M1 line due to the ground-term fine-structure transition ($4f\ ^2F_{7/2} - {}^2F_{5/2}$), which has recently been confirmed experimentally by collaborators in Fudan University using an EBIT [17].

4. Summary

As a concluding remark, the present work demonstrates that observation of faint forbidden-lines from highly ionized heavy elements such as tungsten is feasible at the LHD by using pellet injection techniques. The forbidden lines of the highly ionized heavy elements may provide a new diagnostics mean of core plasmas in visible ranges. Given a spatial distribution of the forbidden-line emission and a corresponding electron temperature profile, it is possible to investigate ion transport effects on the charge state distribution of highly ionized species in the LHD.

EBIT measurements are used to analyze the LHD spectra. Electron density dependence of relative line intensities is an important issue for more precise comparison of the EBIT spectra with those of the LHD plasmas. To this end, collisional-radiative models with detail atomic processes of the tungsten HCIs are being developed.

Acknowledgements

The authors acknowledge all members of the LHD experiment group for their technical supports and fruitful discussions. This work is performed with the support and under the auspices of the NIFS Collaboration Research program (NIFS10KLPF009) and JSPS-NRF-NSFC A3 Foresight Program in the field of Plasma Physics (NSFC: No.11261140328). DK is grateful for a financial support by KAKENHI (23246165).

References

[1] M. B. Chowdhuri et al. Plasma Fusion Res. **2**, S1060, (2007).

[2] T. Putterich et al. Plasma Phys. Control. Fusion **50**, 085016 (2008).

[3] C. S. Harte et al. J. Phys. B: At. Mol. Opt. Phys. **43**, 205004 (2010).

[4] A. E. Kramida and T. Shirai. At. Data Nucl. Data Tables **95**, 305 (2009).

[5] H. Watanabe et al. Phys. Rev. A **63**, 042513 (2001).

[6] A. Komatsu et al. Phys. Scr. T144, 014012 (2011).

[7] H. Watanabe et al. Can. J. Phys. **90**, 497 (2012).

[8] X.-B. Ding et al. J. Phys. B: At. Mol. Opt. Phys. **44**, 145004 (2011).

[9] D. Kato et al. to be published in a topical issue of Phys. Scr. as proceedings of the 16th Int. Conf. on the Phys. of Highly Charged Ions (HCI2012), Heidelberg. Germany, 2 – 7 Sept. 2012.

[10] S. Sudo. J. Plasma Fusion Res. **69**, 1349 (1993).

[11] H. Nihei et al. Rev. Sci. Instrum. **71**, 3747 (2000).

[12] E. Wang et al. Plasma Sci. Tech. **15**, 106 (2013).

[13] A. Komatsu et al. Plasma Fusion Res. **7**, 1201158 (2012).

[14] A. Sasaki. High Energy Density Phys. **9**, 325 (2013).

[15] D. E. Post. J. Nucl. Mater. **220-222**, 143 (1995).

[16] X.-B. Ding et al. Plasma Fusion Res. **7**, 2403128 (2012).

[17] Z. Fei et al. Phys. Rev. A **86**, 062501 (2012).